

On Structural and optical properties of Mn doped ZnO nanopowders

M. Ebrahimizadeh Abrishami

Department of Physics (Materials and Electroceramics Lab.), Ferdowsi University of Mashhad, Iran
ebrahimizadeh@ymail.com

S. M. Hosseini

Department of Physics (Materials and Electroceramics Lab.), Ferdowsi University of Mashhad, Iran
sma_hosseini@yahoo.com

Abstract: $Zn_{1-x}Mn_xO$ ($x=0, 0.02, 0.06, 0.10, 0.15$) nanopowders were synthesized by the sol gel technique calcinated at low temperatures. The solubility of magnetic impurity has been increased and no detectable secondary phases were observed even in the high Mn-doping samples. The phase formation, size and morphology of nanoparticles were investigated using X-ray diffraction, TEM and SEM observations. Optical characterizations, the effect of doping and lattice dynamical parameters were carried out by means of Fourier transform infrared (FTIR) spectroscopy. The optical band gap energy decreases from 3.27 eV to 3.17 eV for pure ZnO and $Zn_{0.98}Mn_{0.02}O$ dispersed powders, respectively.

Keywords: sol gel, ZnO:Mn, nanopowders, optical properties.

1 Introduction

Zinc oxide (ZnO) holds a great position in fabricating the electronic devices due to remarkable electrical and optical properties such as piezoelectricity, controllable conductivity, large band gap energy (3.37 eV), transparency in the visible range and etc [1,2]. Furthermore, ZnO is considered for spintronics applications with magnetic ions (Co, Ni, V, Fe and Mn) doping. In this direction, Mn doped ZnO has become a reasonable choice for Diluted Magnetic Semiconductors (DMS). Even, ferromagnetic state was reported below and above room temperature [3,4]. However, in recent years, synthesis of nanopowders of ZnO, MnO and doping ZnO with transition metals by different routes such as wet chemical methods like sol-gel [5], co-precipitation [6], and combustion [7] in nanotechnology is custom in worldwide.

In this paper, we have synthesized pure and doped ZnO nanopowders via sol gel technique. Effect of Mn doping in lattice parameters were investigated. Transmission spectra in mid-IR region were applied to characterize carefully the influence of Mn on structural properties and determining the refractive index and phonon modes frequencies. In addition, the optical band gap energy was estimated using absorbance spectrum.

2 Experimental procedures

The precursors for the synthesis of $Zn_{1-x}Mn_xO$ ($x=0, 0.02, 0.06, 0.10$ and 0.15) nanoparticles were Zinc acetate dehydrate, $Zn(CH_3COO)_2 \cdot 2H_2O$ (Merck), Manganese acetate tetrahydrate, $Mn(CH_3COO)_4 \cdot 4H_2O$ (Merck), Acetic Acid and Diethanolamine (DEA). Zinc and appropriate amount of manganese acetate were dissolved in a mixture of isopropanol and distilled water by magnetic stirring, heating at 60 °C for 30 minutes. Then the mixture contained Acetic Acid and DEA was added to clear cations solution. The whole solution constantly stirred for 10 min to obtain a clear solution. The molar ratios of Acetic Acid and DEA to cations kept two and unity, respectively. Afterwards, the whole solution with pH=9 was refluxed for 2h at 110 °C to obtain a clear sol. The gel was obtained with the help of heat bath at temperature of 80 °C and then dried at temperatures of 120-150 °C. The resultant powders were calcinated at 500 °C for 1h in air to prepare nanopowders.

Phase identification of nanopowders was analyzed by X-ray diffraction using CuK_{α} radiation ($\lambda=1.5406 \text{ \AA}$). Transmission Electron Microscopy

(TEM, model: LEO 912AB-Germany) and Scanning Electron microscopy (SEM, model: LEO 150-VP-Germany) were used to determine the particle size and morphology of the samples. Optical characterizations were carried out by transmission spectra of powders in KBr matrix in mid-IR region ($4000-200\text{ cm}^{-1}$) and UV absorbance spectra from nanopowders ultrasonically dispersed in distilled water were recorded.

3 Results and discussion

3.1 XRD analysis

The crystal structure, plane orientations and lattice constants were analyzed from XRD patterns as shown in Fig. 1. The crystal structure of $\text{Zn}_{1-x}\text{Mn}_x\text{O}$ ($x=0, 0.02, 0.06, 0.10, 0.15$) was wurtzite with preferred orientation along [101] direction for all samples. Furthermore, XRD spectra revealed mono-phasic structure even in heavy doped nanopowders. This increasing Mn solubility in ZnO structure is due to decreasing particle size, as discussed by Straumal *et al.* [1]. Mn effect on lattice constants and peak positions shifts is presented in Fig. 2. As Mn content increases up to 0.15, the reflection peaks slightly shift to lower angle. Typically, the guidelines in Fig. 1 help us to determine the shifts and the angles related to [101] peaks are mentioned. In fact, increasing the lattice constants (a and c) and the unit cell volume cause the shift in peaks position to lower angles. Because of higher radius of Mn^{2+} (0.66 \AA), in comparison with Zn^{2+} (0.6 \AA), increasing the lattice constants are expectable. However, we observed that the peaks position of $\text{Zn}_{1-x}\text{Mn}_x\text{O}$ shifted towards higher angles. Thus, we concluded that the lattice constants decreased for the following reason. Manganese can also exist in Mn^{3+} , Mn^{4+} in addition to Mn^{2+} . The ionic radii of Mn^{3+} (0.58 \AA) and Mn^{4+} (0.53 \AA) are smaller than Zn^{2+} . In doped ZnO substitution of Zn^{2+} by Mn^{3+} and Mn^{4+} brings about the lattice constant decrease as noted by Bhatti *et al.* [9].

In addition, XRD spectra indicates that Full Width at Half Maximum (FWHM) of [101] peak has decreased with increasing Mn content which is deduced as decreasing particle size, confirmed by Scherrer's relation. SEM and TEM images are shown in Figs 3(a) and 3(b). The average particle size is estimated to be about 30 nm in diameters. The particle size distribution histogram is shown in the inset.

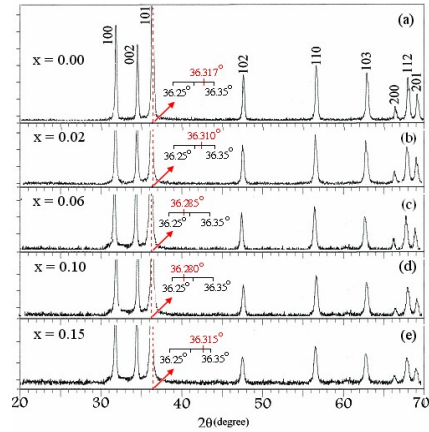


Fig. 1. XRD patterns for $\text{Zn}_{1-x}\text{Mn}_x\text{O}$ (a) $x=0$, (b) $x=0.02$, (c) $x=0.06$, (d) $x=0.10$ and (e) $x=0.15$.

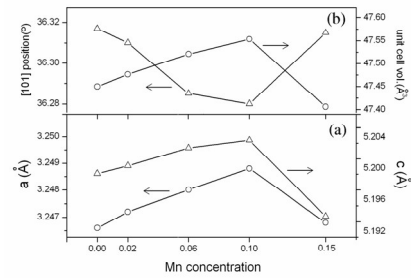


Fig. 2 Structural properties of undoped and doped samples, (a) lattice constants, (b) relation between unit cell volume and angle of [101] peak positions.

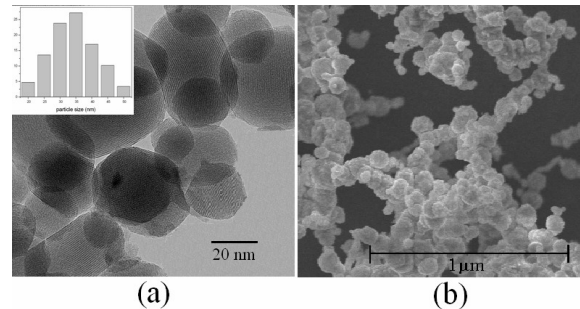


Fig. 3. (a) TEM and (b) SEM image of $\text{Zn}_{0.94}\text{Mn}_{0.06}\text{O}$ nanopowder.

3.2 FTIR analysis

The effect of doping level in FTIR transmission spectra, in the region $4000-200\text{ cm}^{-1}$, is explained in Fig. 4. Zn-O stretching modes are clearly presented in ZnO nanopowder samples centered at about 440 cm^{-1} and a shoulder at 410 cm^{-1} . As presented in this figure, the shoulder is sharpened and blueshifted as Mn content increases. Two guidelines at wavenumbers 410 cm^{-1} and 440 cm^{-1} helps to observe exactly the shoulder shift.

The mid-IR calculated reflectance spectra of pure and doped ZnO nanopowders are shown in Fig. 5.

There is a strong reflection between longitudinal and transversal phonon modes frequencies (ω_{TO} and ω_{LO}), the region reststrahlen. Weak reststrahlen band reflection in $Zn_{1-x}Mn_xO$ is dominated by high free carrier concentration due to heavily doping level. A sharp falling in reflectance spectra around ω_{LO} indicates the semi-insulating system in this region. Also the reststrahlen band becomes wider in doped samples with increasing Mn content up to 0.10 results in more space between phonon modes frequencies. However, this phenomenon acts vice versa in $Zn_{1-x}Mn_xO$ samples. In addition, the high frequencies region is dominated by valence electrons which is observed in fig. 4 that no extra electrons are added to system in doped samples respect to undoped ZnO except in heavily doped ($x=0.10$) nanopowders in which the high frequencies reflectance is remarkably increased. Likewise, we concluded these results as Zn^{2+} ions substitutions by Mn^{2+} and Mn^{3+} ions from XRD analysis.

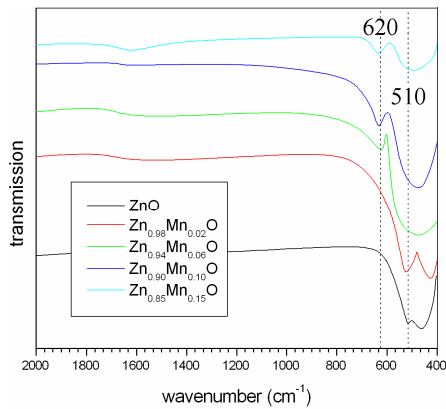


Fig. 4. FTIR spectra of nano- $Zn_{1-x}Mn_xO$ (with $x = 0, 0.02, 0.04, 0.06, 0.10, 0.15$) calculated at $400^\circ C$.

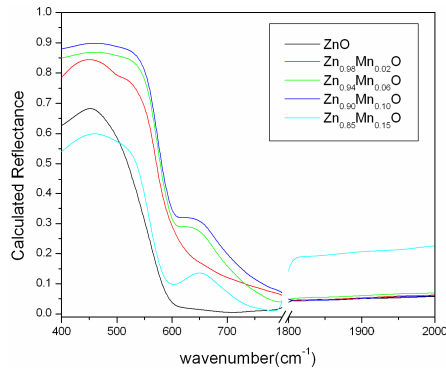


Fig. 5. Calculated reflectance spectra of $Zn_{1-x}Mn_xO$ (with $x = 0, 0.02, 0.04, 0.06, 0.10, 0.15$) calculated at $400^\circ C$.

The dielectric function $\epsilon(\omega)$ in the IR region is controlled by contributions from phonons and free

carriers. We applied the reflectance spectra to calculate the high frequencies dielectric constant $\epsilon(\infty)$ using the relation [10]:

$$\left(\frac{\sqrt{\epsilon_\infty - 1}}{\sqrt{\epsilon_\infty + 1}} \right)^2 = R_\infty \quad (1)$$

where R_∞ is the value of high frequencies reflectance extracted from Fig. 5. Moreover, in the frequency region of $\omega_{TO} < \omega < \omega_{LO}$, the reflectance spectra is maxima and no answer to incident waves exists [10]. Thus, we applied this definition to determine the longitudinal and transversal phonon modes frequencies. The obtained values for $\epsilon(\infty)$ and phonon modes frequencies are summarized in table 1.

Table 1. Lattice-dynamical parameters and high frequency dielectric constant of ZnO and doped nanopowders.

Mn content	$\epsilon(\infty)$	ω_{TO} (cm^{-1})	ω_{LO} (cm^{-1})
0.00	3.51	419	540
0.02	3.50	411	577
0.06	3.57	Out of range	583
0.10	3.56	Out of range	587
0.15	5.19	416	506

3.2 UV analysis

The UV absorbance spectra of pure and Mn-doped ZnO nanopowders are presented in Fig. 6a. A characteristic absorption peak is evident for all UV spectra. As it can be seen, the absorption peaks shift to longer wavelengths as Mn content increases. It must be noted that the absorbance behaviour is completely different from the thin films due to scattering process of the ultraviolet wave from particles dispersed in water.

Since the size of the nanoparticles dispersed in water is much smaller than incident light wavelength, the absorbance spectra are approvable to determine the optical band gap energy, E_g . As shown in Fig. 6b, a reasonable method for extracting band gap energy is investigation of the maxima in first derivative of absorbance with respect to photon energy spectra at the lower energy sides [11]. The band gap decreases from 3.22 eV to 3.12 eV as Mn content increases to $x=0.10$. Decreasing band gap energy with increasing lattice parameters is a well known behaviour as discussed theoretically by Wunderlich *et al.* [12].

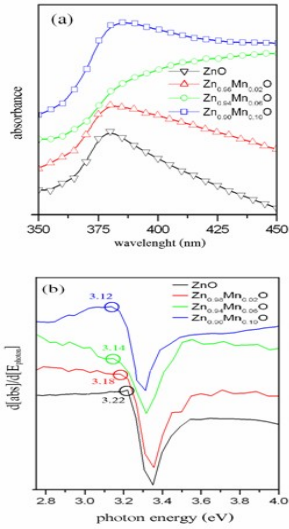


Fig. 6. (a) Optical absorbance spectra of $Zn_{1-x}Mn_xO$ and (b) first derivative of absorbance in terms of photon energy (the band gap energies are circularly marked in the figure)

3 Conclusions

We have presented a synthesis method to achieve single phase Mn-doped ZnO nano-crystals. The solubility of magnetic impurities has been increased by this method. The results indicated irregularities in 0.10 Mn-doped ZnO ceramic nanopowders. The optical properties of the $Zn_{1-x}Mn_xO$ have been investigated from FTIR measurements data in the range of $400-2000\text{ cm}^{-1}$. Lattice constants are increased and the optical band gap energy decreased as Mn concentration rises up to $x=0.10$ in conformity to inverse relation between them. The optical band gap energy decreases from 3.22 eV to 3.12 eV for pure ZnO and $Zn_{0.9}Mn_{0.1}O$ dispersed powders, respectively.

References

[1] M. Ohtaki, K. Araki and K. Yamamoto, "High thermoelectric performance of dually doped ZnO ceramics", *J. Elect. Mater.* 38, 1225-1238, 2009.

[2] S. S. Kwon, W. K. Hong, G. Jo, J. Maeng, T. W. Kim, S. Song and T. Lee, "Piezoelectric effect on the electronic transport characteristics of ZnO nanowire field-effect transistors on bent flexible substrates", *Adv. Mater.* 20, 4507-4512, 2008.

[3] R. K. Singhal, M. Dhawan, S. Kumar, S. N. Dolia, Y. T. Xing, E. Saitovitch, "Room temperature ferromagnetism in Mn doped dilute

ZnO semiconductor; an electronic structure study", *Physica B*, 2009 doi:10.1016/j.physb.2009.07.100.

[4] M. Ebrahimzadeh Abrishami, S. M. Hosseini, E. Attaran Kakhki and A. Kompany, "Characterization of zinc oxide nanopowders doped with MnO", *Mod. Phys. Lett. B*, Accepted, 2009.

[5] Q. Xu, S. Zhou and H. Schmidt, "Magnetic properties of ZnO nanopowders", *J. Allo. and Comp.*, DOI: 10.1016/j.jallcom.2009.08.033.

[6] R. S. Yadav, A. C. Pandey, S. S. Sanjaya, "Optical properties of Europium doped Bunches of ZnO Nanowires Synthesized by coprecipitation method", *Chalcogenide Lett.* 7 223-229, 2009.

[7] N. Riahi-Noori, R. Sarraf-Mamoori, P. Alizadeh and A. Mehdikhani, "Synthesis of ZnO nano powder by a gel combustion method", *J. Ceram. Process. Res.* 9, 257-259, 2009.

[8] B. Straumal, B. Baretzky, A. Mazilkin, S. Protasova, A. Myatiev, P. Straumal, "Increase of Mn solubility with decreasing grain size in ZnO", *J. Europ. Ceram. Soc.* 29, 1973-1976, 2009.

[9] K. P. Bhatti, S. Chaudhary, D. K. Pandya and S. C. Kashyap, "On the room-temperature ferromagnetism in $(ZnO)_{1-x}(MnO)_x$ ", *Solid State Commun.* 136, 385-388, 2005.

[10] N. Peyghambarian, S. W. Koch and A. Mysyrowicz, "Introduction to semiconductor optics", Perentice Hall Int. 1993.

[11] A. E. Morales, E. S. Mora and U. Pal, "Use of diffuse reflectance spectroscopy for optical characterization of un-supported nanostructures", *Revista Mexicana de Fisicas*, 53, 18-22, 2007.

[12] W. Wunderlich, L. Miao, M. Tanemura, S. Tanemura, P. Jin, K. Kaneko, A. Terai, N. Nabatova-Gabin and R. Belkada, "Ab-initio calculations of the optical band-gap of TiO_2 thin films", *Oyo Butsurigaku Kankei Rengo Koenkai Koen Yokoshu*, 01, 765-768, 2004.